

<https://doi.org/10.1038/s42003-024-07381-1>

Metabolic reprogramming of naïve regulatory T cells by IL-7 and IL-15 promotes their persistence and performance upon adoptive transfer



Jessica Filoni^{1,7}, Arianna Ferrari^{1,7}, Tatiana Jofra¹, Anna Rita Putignano², Lorenzo Da Dalt³, Susanna Cesarano⁴, Carla Di Dedda¹, Fabrizia Bonacina³, Federica Marchesi⁵, Giuseppe Danilo Norata³, Chiara Bonini^{4,6}, Lorenzo Piemonti^{1,6} & Paolo Monti¹ ✉

Tregs for adoptive therapy are traditionally expanded *ex vivo* using high doses of IL-2. However, the final Treg product has limited survival once infused in patients, potentially affecting therapeutic effectiveness. Here, we tested a novel expansion protocol in which highly purified naïve Tregs were expanded with a combination of IL-7 and IL-15, in the absence of IL-2. The final Treg product was enriched with cells displaying an immature CD45RA⁺CD62L⁺CD95⁺ phenotype, reminiscent of conventional memory stem T cells. The combination of IL-7 and IL-15 confers Tregs a glycolytic metabolism and improved metabolic fitness, characterized by an increased capacity to adapt metabolism according to glucose and oxygen availability. Tregs expanded with IL-7 and IL-15 showed longer persistence and an improved capacity to control xeno-GvHD in NSG mice. This work suggests that metabolic reprogramming induced by IL-7 and IL-15 provides better Treg performance for adoptive therapy.

CD4⁺CD25^{bright}CD127^{low}FOXP3⁺ regulatory T cells (Treg) represent an immune cell subset specialized in the control of immune response and induction of immunological tolerance through a broad arsenal of contact-dependent and -independent suppressive mechanisms^{1–3}. More than 50 active or completed clinical trials are exploring the potential of adoptive Treg therapy, to achieving localized and specific immune suppression to control transplant rejection⁴, graft vs host disease⁵, and autoimmunity⁶. Clinical trials testing administration of polyclonal Tregs in recent-onset T1D have observed an excellent safety profile but limited efficacy^{7,8}, underlying several barriers to achieve therapeutic effectiveness. One barrier is the lack of antigen specificity of polyclonal Tregs. The emergence of advanced gene transfer and genome editing technologies offer a promising solution to this challenge by enabling the precise modification of Treg cells to express chimeric antigen receptors (CARs) or T cell receptors (TCRs) with specificity to antigens⁹. A second critical aspect is the need to maintain Treg number and function overtime to control T cell responses¹⁰. This is evident from clinical trials which have shown difficulties in generating

sufficient Treg cells in some patients, coupled with a rapid decline in Treg numbers after infusion. Specifically, Bluestone et al. detailed this decline as a two-phase exponential process, where a predominant subset of Tregs (75–90%) exhibited a rapid reduction in numbers, with a half-life spanning just a few days. Conversely, a smaller fraction of Tregs (10–25%) demonstrated longevity, remaining detectable for up to one year following infusion⁸. Interestingly, the surviving Tregs displayed a CCR7⁺CD45RA⁺CD45RO^{-/+} phenotype, which is similar to the one of less differentiated naïve or memory stem T cells¹¹. A specific need to generate enough Tregs with optimal survival potential is therefore a critical step to achieve therapeutic efficacy. Current protocols for generation of Tregs for adoptive transfer include isolation of polyclonal Tregs from peripheral blood and *in vitro* expansion using anti CD3/CD38 microbeads in combination with high doses IL-2^{12,13}. However, Tregs can proliferate also in response to homeostatic cytokines such as IL-7^{14,15}. Despite low expression of the IL-7R α (CD127)¹⁶, IL-7 triggers proliferation of human CD45RA⁺ naïve Tregs, but not CD45RA⁻ memory Tregs *in vitro*¹⁷. Furthermore, in patients

¹San Raffaele Diabetes Research Institute, IRCCS Ospedale San Raffaele Milan, Milan, Italy. ²Department of Immunology and Inflammation, IRCCS Humanitas Research Hospital Rozzano, Rozzano, Italy. ³Department of Pharmacological and Biomolecular Sciences, Università degli Studi di Milano, Milan, Italy. ⁴Experimental Hematology Unit, IRCCS Ospedale San Raffaele Milan, Milan, Italy. ⁵Department of Medical Biotechnology and Translational Medicine, University of Milan, Milan, Italy. ⁶Vita-Salute San Raffaele University, Milan, Italy. ⁷These authors contributed equally: Jessica Filoni, Arianna Ferrari. ✉e-mail: monti.paolo@hsr.it

treated with the anti-CD25 monoclonal antibody basiliximab, IL-7 contributes to the reconstitution of the Treg compartment¹⁸. In our latest work, we demonstrated that by expanding naïve Tregs with both IL-2 and IL-7, we can maintain their CD45RA⁺ phenotype and increase their resistance to apoptosis, leading to enhanced durability in NSG mice¹⁹. However, this approach did lead to a lower overall yield of cells and a diminished suppressive ability when IL-7 was included. We now introduce an innovative expansion method where naïve Tregs are expanded using a combination of IL-7 and IL-15, without IL-2, which significantly enhances Treg expansion, their suppressive function, longevity, and effectiveness in an NSG mouse model of xeno-GvHD.

Results

Expansion with IL-7 plus IL-15 improves final cell yield, viability and suppressive function

We have previously shown that naïve Tregs are capable of proliferating in response to IL-7, even though they exhibit low levels of the IL-7 receptor alpha chain (CD127)¹⁷. To set up an expansion protocol based on a combination of IL-7 and IL-15 we further investigated the expression and functionality of the IL-15 receptor alpha chain (CD215) on Tregs.

Compared to CD4⁺ conventional T cells (Tconvs), Treg cells express lower levels of CD215 (Mean Fluorescence Intensity, MFI: 1148 ± 178 Tregs vs 2819 ± 226 Tconvs, *n* = 4, *P* = 0.002) (Fig. 1A, left panel). We classified Tregs subsets, according to the expression of CD45RA, CD62L and CD95²⁰, into naïve Tregs (Treg-n; CD45RA⁺CD62L⁺CD95⁻), stem cell memory Tregs (Treg-scm; CD45RA⁺CD62L⁺CD95⁺), central memory Tregs (Treg-cm; CD45RA⁻CD62L⁺CD95⁺), effector memory Tregs (Treg-em; CD45RA⁻CD62L⁻CD95⁺) and Treg effector memory re-expressing CD45RA (Treg-emra; CD45RA⁺CD62L⁻CD95⁺). We observed a sequential reduction in CD215 expression starting Treg-n (MFI = 2620 ± 344) through to Treg-scm (MFI = 1880 ± 304), Treg-cm (MFI = 1582 ± 227), Treg-em (MFI = 922 ± 227), and finally Treg-temra, (MFI = 623 ± 134) (Fig. 1A, right panel). Similarly, Tconvs exhibit CD215 expression across their subsets following a comparable pattern, although the trend of decreasing expression from Tn to Temra subsets was less pronounced. To test the responsiveness of Tregs to IL-15, we stimulated Tregs with IL-15 (10 ng/ml) and investigated STAT-5 phosphorylation. Reflecting the expression of CD215, Treg cells exhibited a lower degree of STAT-5 phosphorylation compared to Tconv cells (pSTAT-5 MFI: 1567 ± 464 for Treg vs 3539 ± 666 for Tconv, *n* = 4, *P* = 0.003) (Fig. 1B, left panel). When

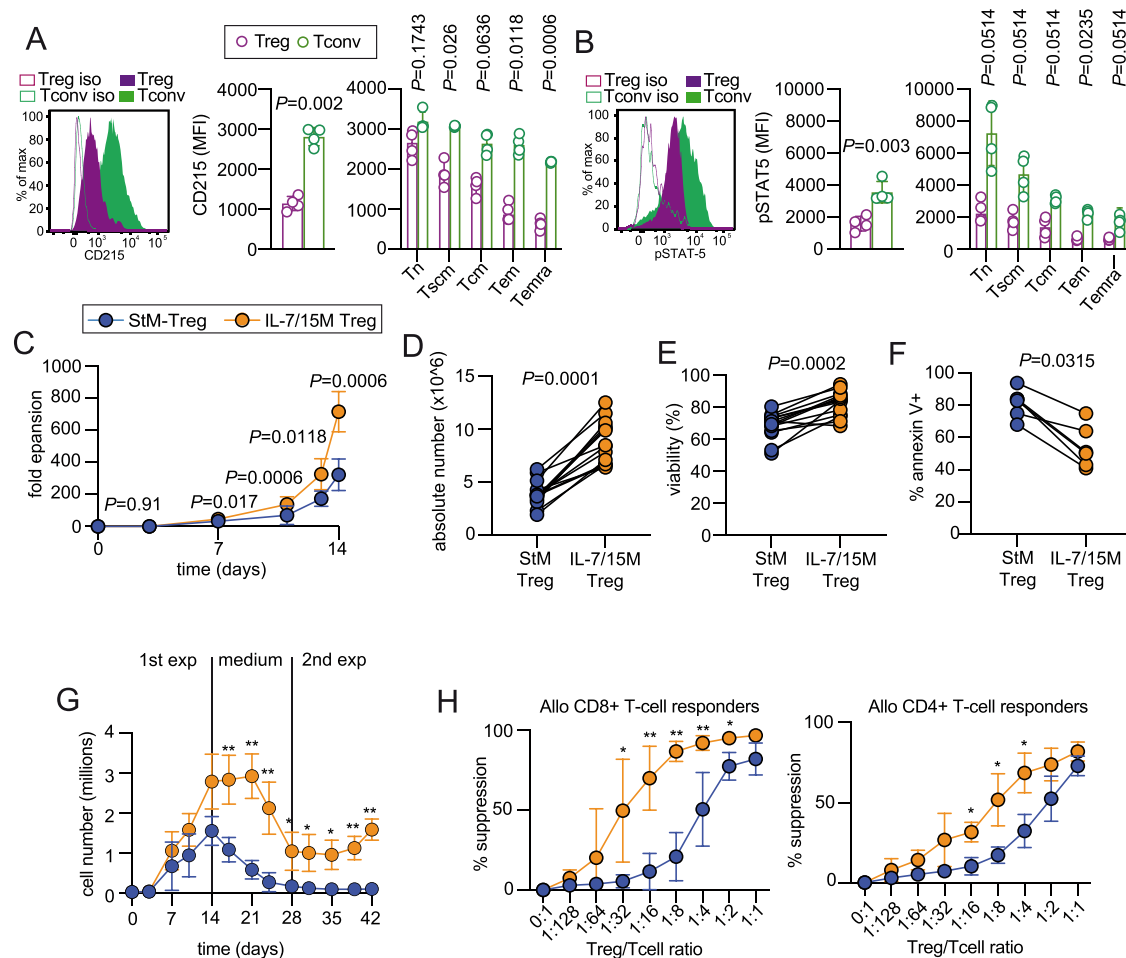


Fig. 1 | Treg express a functional IL-15 receptor alpha chain (CD215) and proliferate in response to a combination of IL-7 and IL-15. A Representative FACS plot showing the expression of CD215 in gated Treg (CD4⁺CD25^{bright}CD127^{low}) and Tconv (CD4⁺CD25^{low}CD127^{high}) from a PBMC sample. The graph (right panel) shows the mean fluorescence intensity (MFI) of CD215 in Treg and Tconv classified as naïve and memory subsets (*n* = 4). **B** Representative FACS plot of phosphorylated STAT-5 after 1 min of incubation of Treg and Tconv with 10 ng/ml of rhIL-15. The graph (right panel) shows the MFI of phospho-STAT-5 in Treg and Tconv divided into naïve and memory subsets after incubation with IL-15 (*n* = 4). **C** Fold expansion of StM-Treg and IL-7/15M-Treg. **D** Final cell yield of StM-Treg and IL-7/15M-Treg.

E Viability measured as trypan blue exclusion of StM-Treg and IL-7/15M-Treg. **F** Percentage of annexin V⁺ cells after apoptosis induction with an agonistic anti fas antibody in StM-Treg and IL-7/15M-Treg. **G** Changes in the number of viable cells after first expansion, contraction due to withdrawal of cytokines and microbeads, and secondary expansion of residual cell. **H** Percentage of suppression of proliferation of CD8⁺ (upper panel) and CD4⁺ (lower panel) allogenic T cells at different Treg/Tcell ratios. The Wilcoxon matched paired *t*-test with the Dunn–Bonferroni post hoc test was used for comparisons. **P* < 0.05, ***P* < 0.01, ****P* < 0.001, ns, *P* > 0.05.

analyzed according to naïve and memory subsets, a decreasing pattern in STAT-5 phosphorylation was noted ranging from Treg-n (MFI = 2361 ± 703), through Treg-scm (MFI = 1760 ± 537), to Treg-cm (MFI = 1355 ± 611), Treg-em (MFI = 648 ± 127), and finally Treg-emra (MFI = 639 ± 95) (Fig. 1B, right panel). In comparison, p-STAT-5 levels among Tconv subsets followed a similar downward trend. Based on these and previously published results¹⁹ we set up an expansion protocol in which FACS sorted CD45RA⁺CD62L⁺ Treg-n and Treg-scm (Fig. S1A) were cultured with anti CD3/CD28 microbeads (1:1 ratio with cells) for 14 days in the presence of IL-7 (10 ng/ml) and IL-15 (10 ng/ml). The standard method for Treg expansion is similar but with 300UI/ml of IL-2 instead of IL-7 and IL-15. Treg expanded through the standard method were referred as StM-Treg, whereas those expanded via the newer IL-7 and IL-15 technique were named IL-7/15M-Treg. The fold expansion curve showed a greater fold expansion of IL-7/15M-Treg (14 days fold expansion: 323 ± 98 StM vs 716 ± 126 IL-7/IL-15M, *n* = 14, *P* = 0.0025) (Fig. 1C). The final cell yields after expansion starting from 8500-17400 sorted Treg (detail of each Treg isolation in Fig. S1B) were greater for IL-7/15M-Treg than StM-Treg (mean ± SD: 3.905.000 ± 1183587 StM vs 8.751.667 ± 2.008.551 IL-7/IL-15M, *n* = 14, *P* = 0.0001) (Fig. 1D). Cell viability measured on day 14 by trypan blue staining exclusion assay was higher for IL-7/15M-Treg than StM-Treg (% viable cells mean ± SD: 68 ± 8 StM vs 82 ± 8 IL-7/IL-15M, *n* = 14, *P* = 0.0002) (Fig. 1E).

Previously, we demonstrated that incorporating IL-7 into an IL-2 based Treg expansion protocol enhances the resistance of expanded Tregs to apoptosis¹⁹. Therefore, we sought to determine resistance to apoptosis in both StM-Tregs and IL-7/15M-Tregs. Initially, we applied direct apoptotic stimulus by treating the cells with an agonistic anti-fas monoclonal IgM antibody for 24 hours. The proportion of cells undergoing apoptosis, as determined by the expression of annexin V, was significantly lower in IL-7/IL-15M-Tregs as compared to StM-Tregs (% annexin V⁺: 81.3 ± 8.9 StM vs 54 ± 13 IL-7/IL-15M, *n* = 6, *P* = 0.0315) (Fig. 1F). Subsequently, we performed experiments to test the resistance of expanded Tregs to the withdrawal of cytokines and stimuli, a condition that is likely to happen when in vitro expanded Tregs are injected in patients. After 14 days of expansion in the presence of cytokines, we cultured Tregs for additional 14 days in the absence of cytokines or TCR triggering signals, while monitoring changes in the number of viable cells (absolute number of trypan blue negative cells) every 3 days. Under these conditions, viable StM-Tregs immediately started to decline, with a loss of 87 ± 11% of viable cells from day 14 to day 28 (Fig. 1G). In contrast, viable IL-7/15M-Tregs remained stable for the first week and declined between day 21 and day 28 with a loss of 63 ± 11% in viable cells, indicating enhanced survival ability under conditions of growth factor deprivation. Notably, when antiCD3/CD28 microbeads and cytokines were added back to the culture at day 28, only IL-7/15M-Treg retained a capacity to re-expand.

Suppression of conventional T cell proliferation is a hallmark of Treg function. To determine the suppressive capacity of expanded Treg, both StM-Treg and IL-7/15M-Treg were tested in a suppression assay against allogenic CD8⁺ and CD4⁺T cells stimulated with antiCD3/CD28 microbeads. IL-7/15M-Treg displayed an increased suppressive function, which was particularly significant at lower Treg to Tconv ratios (Fig. 1H). To determine whether Treg retain suppressive capacity after withdrawal of cytokines and the CD3/28 stimuli, both StM-Treg and IL-7/15M-Tregs were cultured in fresh medium for 5 days and then tested in a suppression assay. Even after withdrawal of cytokines and the CD3/28 stimuli IL-7/15M Treg were more suppressive than StM-Treg (Supplementary Fig. 1C).

Treg expansion with the IL-7/IL-15M preserves an immature phenotype and promotes a glycolytic metabolism

We compared the relative proportion of naïve and memory subsets of StM-Tregs and IL-7/IL-15M-Tregs. After 14 days of expansion starting from sorted CD45RA⁺CD62L⁺ Tregs, the large majority of StM-Tregs lost the expression of CD45RA, whereas the proportion of CD45RA⁺ Tregs was very high in IL-7/15M-Treg (Fig. 2A). Comparing the relative proportion of

naïve and memory subsets, IL-7/15M-Tregs were enriched in Treg-n (% of CD45RA⁺CD62L⁺CD95⁺: 4 ± 2 StM vs 11 ± 2 IL-7/IL-15M, *n* = 9, *P* = 0.036), and Treg-scm (% of CD45RA⁺CD62L⁺CD95⁺: 4 ± 2 StM vs 29 ± 8 IL-7/IL-15M, *n* = 9, *P* = 0.0039), have similar percentage of Treg-cm (% of CD45RA⁺CD62L⁺CD95⁺: 24 ± 12 StM vs 39 ± 6 IL-7/IL-15M, *n* = 9, *P* = 0.21) and Treg-temra (% of CD45RA⁺CD62L⁺CD95⁺: 8 ± 6 StM vs 4 ± 3 IL-7/IL-15M, *n* = 9, *P* = 0.21), and showed reduced percentages of Treg-em (%: 60 ± 16 StM vs 17 ± 9 IL-7/IL-15M, *n* = 9, *P* = 0.0039) (Fig. 2B). RNAseq analysis of StM-Treg and IL-7/15M-Treg on day 14 of expansion (Fig. S2A) revealed comparable levels of expression across a fundamental set of genes that define the Treg signature (Fig. 2C). Additionally, the analysis indicated similar levels of expression for transcription factors that are critical for defining T cell subsets, including elevated levels of FOXP3 (characteristic of Tregs) and lower levels of TBX21 (Th1), GATA3 (Th2), and RORC (Th17). This suggests a consistent stability in the Treg phenotype between both groups (Fig. 2D). A phenotypic analysis conducted by flow cytometry showed similar expression of FOXP3 (Fig. S3A). Interestingly, IL-7/15M-Tregs expressed a set of genes forming a distinct signature compared to that of StM-Tregs (Figs. 2E and S2C). This unique signature was further analyzed in comparison to one identified by Motwani et al. for Tregs derived from cord blood²¹. By employing the ssGSEA algorithm, we assessed the enrichment score of this signature across samples, revealing that IL-7/15M-Treg signature more closely resembled that of cord blood-derived Tregs rather than Tregs derived from adult peripheral blood, (Fig. 2F). Notably, pathways associated with cell fate commitment were enriched in StM-Treg (Fig. S2B), suggesting that IL-7/15M-Tregs maintained a less differentiated, more immature state post-expansion. Overall, these data support the concept that IL-7 and IL-15 foster Treg expansion, bypassing the differentiation-inducing effects of IL-2.

The unique genetic signature distinguishing IL-7/15M-Treg from StM-Treg featured genes essential for cellular bioenergetics processes, such as Glut1, Glut3, hexokinase 1, and hexokinase 2 (Fig. 2E). To have a better insight into differences in bio-energetic metabolism we examined RNAseq data, focusing on genes coding for enzymes and molecules involved in metabolic pathways, to compare their expression levels in IL-7/15M-Treg and StM-Treg. IL-7/15M-Treg displayed an up-regulation of genes involved in glycolysis and sterol metabolism, whereas the expression of genes involved in fatty acid oxidation (FAO) and oxidative phosphorylation (OXPHOS) was reduced (Fig. 2G).

Treg expansion with the IL-7/15M improves metabolic fitness

To directly determine the metabolic capacities and dependencies of Treg after expansion, we utilized SCENITH (single-cell energetic metabolism by profiling translation inhibition) technology²², adapted to our flow cytometry panel. The SCENITH is based on the finding that half of the total ATP generated from the breakdown of glucose, lipids and amino acids is immediately consumed by the protein synthesis (PS)²³, offering the possibility to measure PS levels (measured through puromycin incorporation) as a surrogate marker of the global ATP production of a cell²⁴. Changes in PS levels induced by the addition of selective metabolic inhibitors, such as 2-deoxy-glucose or oligomycin, revealed which and to which extent a metabolic pathway was providing ATP to the cell (Fig. S4A). This technique assesses the reliance of cells on glucose and mitochondrial processes, as well as glycolytic capacity and fatty acid/amino acid oxidation capacity as derived parameters, providing insight of the metabolic pathways used by a cell to provide ATP for protein synthesis. SCENITH analysis revealed that IL-7/15M-Tregs exhibited reduced dependence on glucose and mitochondria, leading to an increased capacity for fatty acid oxidation(FAO)/amino acid oxidation (AAO) and glycolysis compared to StM-Tregs (Fig. 3A). Corroborating these findings, the dynamic uptake of the fluorescent glucose analog 2NBDG was higher in IL-7/15M-Tregs than in StM-Tregs (AUC: StM-Treg 1.72 × 10⁶ vs IL-7/15M-Treg 2.69 × 10⁶) (Fig. 3B). Moreover, we detected an increased lactate concentration in the supernatant of IL-7/15M-Tregs (mMol/ml: StM-Treg 34 ± 12 vs IL-7/15M-Treg 80 ± 19, *n* = 6, *P* = 0.035) casting for increased anaerobic glycolysis (Fig. 3C). To assess

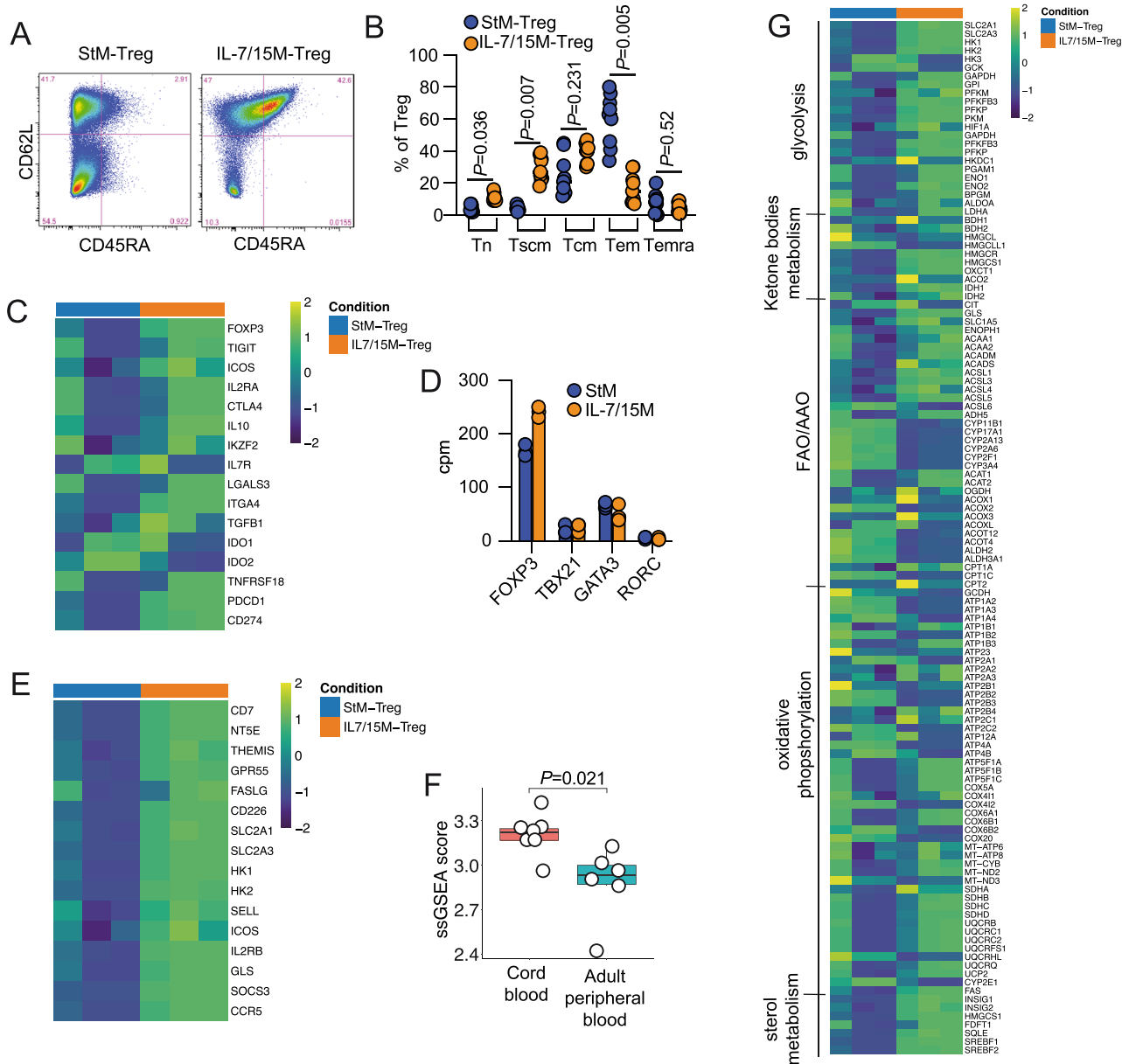


Fig. 2 | IL-7/15M-Treg preserves an immature phenotype and display a distinct gene expression profile. **A** Representative FACS plot showing the expression of CD62L and CD45RA in StM-Treg and IL-7/15M-Treg. **B** Percentage of StM-Treg and IL-7/15M-Treg with a Tn, Tscm, Tcm, Tem and Temra phenotype. **C** Expression of genes that defines the Treg subset in StM-Treg and IL-7/15M-Treg. **D** Expression of genes coding for transcription factor FoxP3, T-bet, Gata4 and Ror-

gamma-C. **E** Expression of genes that were differentially expressed between StM-Treg and IL-7/15M-Treg. **F** ssGSEA enrichment score of the signature of IL-7/15M-Treg (**E**) in Treg isolated from cord blood and adult peripheral blood. **G** Expression of genes involved in metabolic pathways. The Wilcoxon matched paired *t*-test with the Dunn–Bonferroni post hoc test (**B**) or Wilcoxon Rank Sum test (**F**) were used for comparisons.

variations in mitochondrial mass among expanded Treg populations, cells were labeled with MitoGreen dye and analyzed, comparing them to Treg immediately post-sorting. We found a substantial and similar increase in the mitochondrial cell mass from freshly sorted Tregs to expanded StM-Tregs and IL-7/IL-15M-Tregs (Fig. 3D). However, using confocal microscopy to study the number and morphology of mitochondria we found that StM-Tregs possessed fewer but larger mitochondria, whereas IL-7/IL-15M-Tregs exhibited an increased quantity of smaller mitochondria, suggesting a different plasticity that may reflect ongoing processes of mitochondrial fission related to changes in mitochondrial respiration (Fig. 3E).

The improved energetic phenotype of in vitro cultured IL-7/15M-Treg over StM-Treg cells was also confirmed by Seahorse analysis. Taking advantage from Real-Time ATP rate assay, we detected an increased oxygen

consumption rate (OCR) and extracellular acidification rate (ECAR) in IL-7/15M-Treg compared to StM-Treg (Fig. 3F, G). This difference, however, becomes less pronounced upon partial inhibition of mitochondrial respiration. Specifically, when mitochondrial function was dampened with oligomycin, an inhibitor of ATP synthase (complex V), and further with the combination of rotenone and antimycin A, which inhibit complexes I and III respectively, the difference in the metabolic profiles between the two Treg subsets was partially diminished (Fig. 3F). Instead, glycolytic flux, determined following ECAR measurement, was further increased in IL-7/15M-Tregs following the inhibition of mitochondrial function (Fig. 3G), suggesting that the energetic advantage of IL-7/15M could primarily result from an enhanced glucose metabolism through glycolysis, fulfilling the energy demands of these highly proliferative cells. Extrapolation of these data

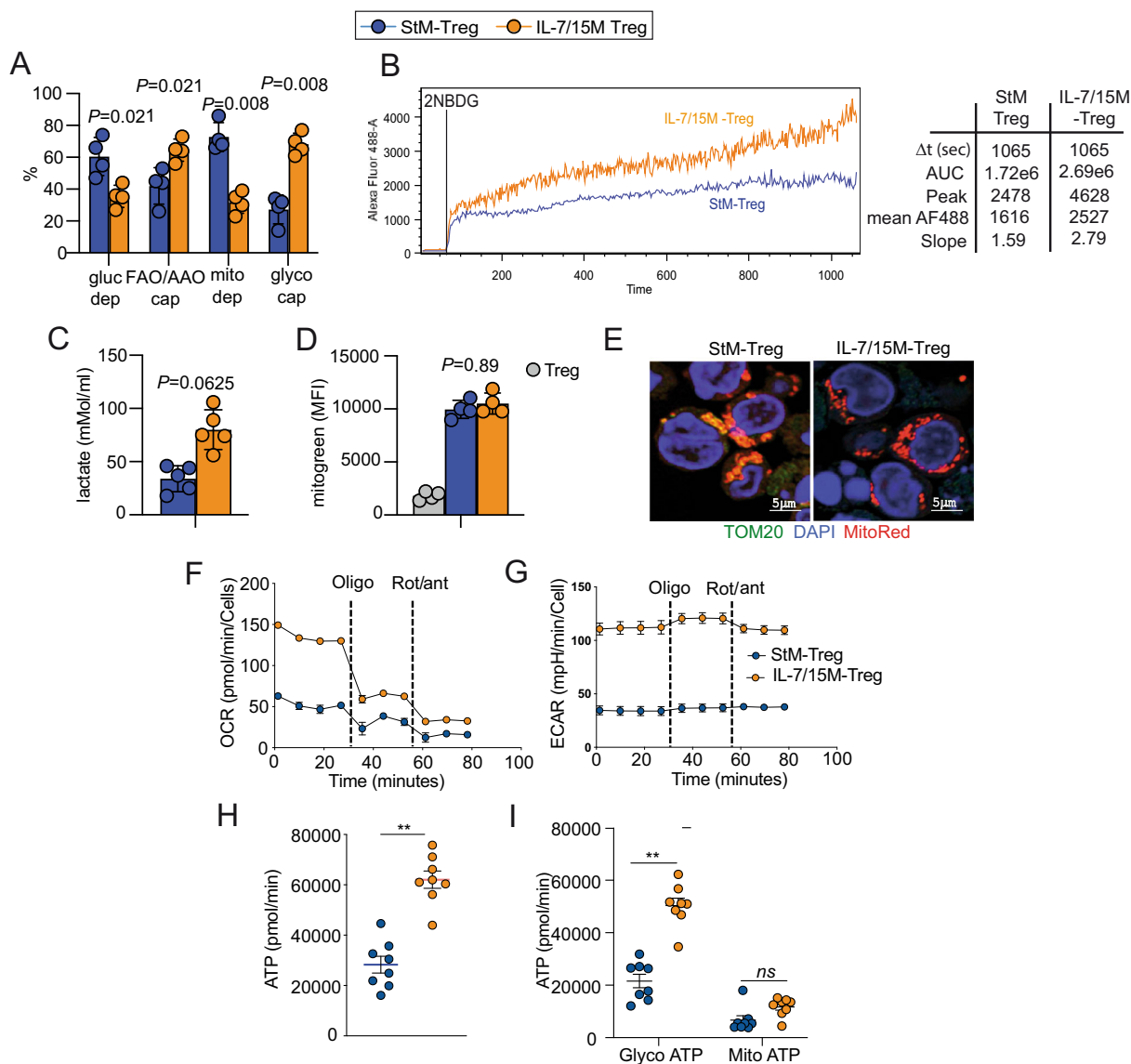


Fig. 3 | IL-7/15M-Treg display an efficient metabolism based on glycolysis.
A Glucose and mitochondrial dependencies and relative FAO/AAO and glycolytic capacities in StM-Treg and IL-7/15M-Treg after 14 days of in vitro expansion.
B Dynamic uptake of the fluorescent glucose analog 2NBDG in StM-Treg or IL-7/15M-Treg. Parameters of the two curves were calculated and compared.
C Lactate concentration (mMol/ml) in the supernatant of 106 StM-Treg or IL-7/15M-Treg cultured for 24 h.
D Mitochondrial mass measured as fluorescence of the MitoGreen dye in freshly isolated Treg and in StM-Treg or IL-7/15M-Treg. The Wilcoxon matched paired *t*-test (**A–D**) was used for comparisons.
E Confocal images showing

the shape of mitochondria in StM-Treg and IL-7/15M-Treg after 14 days of in vitro expansion. **F** Oxygen consumption rate (OCR) and **G** extracellular acidification rate (ECAR) in StM-Treg and IL-7/15M-Treg measured by Seahorse technology at basal and after the injection of oligomycin (1.5 μM) and a mixture of rotenone and antimycin (0.5 μM each). **H** Total ATP production and **I** ATP produced by glycolysis (Glyco ATP) and oxidative phosphorylation (Mito ATP) measured by Seahorse technology with the real-time ATP rate assay. Data are presented as mean ± SEM, *n* = 8/group; statistical analyses were performed by *t*-test (**H**) and two-way Anova (**I**). ***P* < 0.01, ns *P* > 0.05.

clearly showed a significantly increased production of ATP from IL-7/15M-Tregs compared to StM-Tregs (Fig. 3H), that was mainly derived by glycolysis over oxidative phosphorylation (Fig. 3I).

IL-7/IL-15-Tregs survived longer and delayed the onset of xeno-GvHD in the NSG mice

To test Treg survival and suppressive performances in vivo, we used a model of xenogeneic graft-versus-host disease (xeno-GvHD). In this model, NSG mice were co-transplanted with autologous human peripheral blood mononuclear cells (PBMC) and green fluorescent protein (GFP)-transduced Treg cells, allowing for the tracking of these two populations over time. Moreover, we monitored the onset and the severity of GvHD symptoms according to a specific scoring system (refer to Fig. S4B) alongside monitoring weight loss. Both IL-7/15M-Tregs and StM-Tregs expanded

in vivo right after infusion showing a spike of circulating cells after approximately 7 days (Fig. 4A). This spike was followed by a contraction phase in which StM-Tregs progressively disappeared from the circulation. In contrast, IL-7/15M-Tregs stabilized after the contraction phase and remained detectable in all mice until the end of the experiment (35 days post infusion). In the absence of Treg cells, conventional T cells present in the PBMC rapidly expanded in NSG mice (Fig. 4B), leading to early onset GvHD symptoms (Fig. 4C) and significant weight loss (Fig. 4D). IL-7/15M-Tregs were more efficient than StM-Tregs in controlling the expansion of Tconvs (Fig. 4B) as well as the onset and severity of GvHD symptoms (Fig. 4C) and weight loss (Fig. 4D). The overall survival rates significantly favored mice treated with IL-7/15M-Tregs over those treated with StM-Tregs (*P* = 0.0389) (*P* = 0.0389) (Fig. 4E). The experiment was terminated on day 35 and liver and spleen were collected from survivals. Mice treated

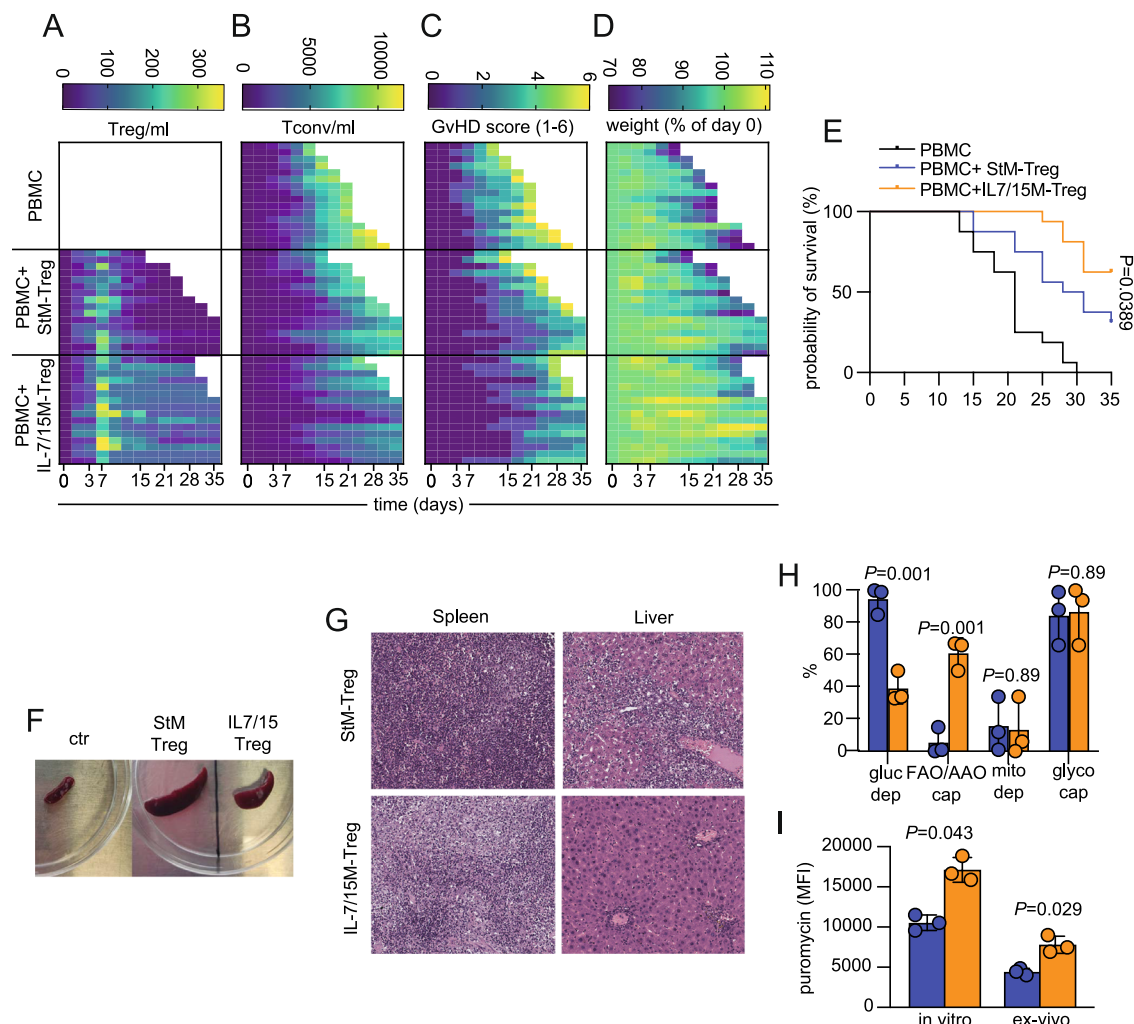


Fig. 4 | IL-7/15-Treg persist longer in NSG mice and are more protective against xeno-GvHD. Heatmaps showing **A** GFP+Treg (number/ml), **B** CD3+ Tconv (number/ml), **C** GvHD score (1–6, Supplementary Table 4B) and **D** weight (% relative to day 0) in NSG mice infused with 10^7 PBMC and 5×10^6 Treg. **E** Kaplan–Meier survival curve comparing NSG mice receiving human PBMC alone or in combination with expanded Tregs (16 animals for each group). Statistical analysis was performed using the Log-rank (Mantel–Cox) test. **F** Pictures

of spleens collected from untreated, StM-Treg- and IL-7/15-Treg-treated mice NSG mice. **G** Representative H&E in tissue sections obtained from spleen and liver of treated mice at day 35. **H** Glucose and mitochondrial dependencies and relative FAO/AAO and glycolytic capacities in StM-Treg and IL-7/15M-Treg retrieved from NSG mice spleen 7 days after injection. **I** Puromycin fluorescence in StM-Treg and IL-7/15M-Treg both after 14 days of in vitro expansion, and 7 days after injection in NSG mice. The Wilcoxon matched paired *t*-test (**A–D**) was used for comparisons.

StM-Tregs developed marked splenomegaly compared to mice treated IL-7/15M-Tregs and non-transplanted NSG mice (Fig. 4F). Immunohistochemistry showed an increased lymphocyte infiltration in both spleen and liver from mice infused with StM-Treg as compared to mice infused with IL-7/15M-Treg (Fig. 4G).

We took advantage of the NSG mouse model also to study metabolism of Treg in vivo. We showed the Treg metabolic signature (Fig. 3) of cells at the end of a 14 days expansion in vitro, using medium with 17 mM glucose, under conditions maintaining 21% oxygen. Once Tregs are introduced into patients, these in vitro conditions undergo significant changes, with glucose concentrations varying between 1 to 5.5 mM and oxygen partial pressures ranging from 1 to 12% across different tissues. To explore how the shift from an in vitro environment to an in vivo one might impact the metabolic behavior of Tregs, we administered expanded Tregs into NSG mice and, seven days later, harvested them from the spleen to analyze their metabolic functions and needs ex vivo through the SCENITH method. After 7 days in NSG mice, IL-7/IL-15-Tregs continued to exhibit a lesser dependency on glucose compared to their initial state, while the opposite was true for StM-Tregs which also presented higher FAO/AAO capacity (Fig. 4H). Interestingly, both IL-7/15-Tregs and StM-Tregs displayed extremely low

mitochondrial dependence and, consequently, an extremely high glycolytic capacity. Puromycin fluorescence (MFI) was also evaluated as an indirect indicator to assess the overall capacity of the Treg metabolic machinery to sustain protein synthesis. IL-7/15-Tregs showed a higher puromycin MFI than StM-Tregs after in vitro expansion, in line with a more active metabolism (Fig. 4I). Despite a striking reduction of puromycin fluorescence in Tregs after infusion in NSG mice, IL-7/15-Tregs continued to display a higher puromycin MFI than StM-Tregs, indicating a metabolic advantage also in the in vivo milieu.

Discussion

Adoptive transfer of Treg holds therapeutic promise in controlling immune responses and restoring peripheral tolerance in transplantation, GVHD, and autoimmune diseases. However, recent clinical trials have shown that in vitro expanded Tregs have a limited capacity to persist in patients, thus limiting the therapeutic effectiveness of Treg therapy. Efforts to prolong survival of expanded Treg by administration of exogenous IL-2 did not prove significant benefits, also adding the risk of expanding other cell subsets such as CD8+ T cells²⁵. Our study has focused on using homeostatic cytokines IL-7 and IL-15 during in vitro expansion to generate Treg that

better adapt to the *in vivo* environment. Our approach stems from our previous observations that naïve Treg proliferate in response to IL-7 both *in vitro*¹⁷ and *in vivo* in patients¹⁸. Building on this, we previously developed a Treg expansion protocol that combined IL-2 with IL-7, which showed advantages in enhancing resistance to apoptosis and stress, albeit with compromises in cell yield and suppressive capacity¹⁹. In the current study, we report that naïve Treg can be effectively expanded using a novel combination of IL-7 and IL-15, in the absence of IL-2.

The expansion of Treg for adoptive transfer traditionally relies on high doses of IL-2, eventually generating a high number of Treg comprising short-lived Treg *in vivo*, alongside a long-lived subset capable of persisting for more than a year⁸. While the addition of IL-7 increases the content of CD45RA⁺ long-lived Treg, this cytokine alone provides only a modest proliferative signal. This limited effect may be attributed to the low expression of the IL-7 receptor alpha (CD127), rendering IL-7 insufficient for a standalone option in Treg expansion protocols. However, IL-7 is a homeostatic cytokine with limited ability to induce proliferation even in CD127^{high} conventional T cells²⁶. We observed that Tregs robustly express the IL-15 receptor alpha, which could drive a vigorous proliferation in response to a combination of IL-7 and IL-15, resulting in a greater fold expansion, final increasing cell yield with improved viability. We observed that the final Treg product was enriched in Treg still expressing CD45RA, CD62L and CD95 a phenotype reminiscent of that of conventional memory stem T cells. A combination of IL-7 and IL-15 is used also to generate conventional T cells with a memory stem cell phenotype from naïve precursors²⁶.

The preservation of an immature phenotype in expanded Tregs is critical for achieving extended survival times in patients. Best estimates for the average lifespans of human T cells suggest that a naïve phenotype is clearly associated with a longer lifespan. Deuterium labeling experiments demonstrated that CD45RA⁺ naïve CD4⁺ and CD8⁺ T cells have a lifespan of 2.4 and 2.8 years, respectively^{27,28}. In contrast, their memory CD45RO⁺ counterparts have a lifespan of approximately 0.5 years. Although similar deuterium labeling studies on Tregs are scarce, available data suggest that endogenous memory CD45RO⁺ Tregs undergo rapid turnover, with a lifespan of just 12 days²⁹. Singh et al. took on the challenge of evaluating the pharmacokinetics of therapeutic Treg cells in rhesus macaques, showing that infused Treg precipitously disappeared from circulation with half-lives of 32 h in the first phase and 120 h in the second phase³⁰. While there are no available data on the lifespan of endogenous naïve Treg in humans, Tang et al. showed that Treg that survive longer in patients undergoing Treg adoptive transfer display a CD45RA⁺ CCR7⁺ phenotype⁸. This suggests that a naïve-like phenotype of expanded Treg can confer longer lifespan. However, a further consideration has to be done with respect to our ability to prolong Treg lifespan. Even though it is possible to improve Treg persistence, their biological lifespan is remarkably short, potentially limiting our efforts to generate Treg product that persist for years in patients. Providing multiple infusion of expanded Treg needs to be considered as an option to obtain a therapeutic effect.

The enhanced efficacy observed in Treg cells expanded with IL-7 and IL-15 is tied to their superior metabolic health, primarily characterized by a strong reliance on glycolysis for energy production. In line with this, it has been shown that freshly isolated human Treg exhibited a more glycolytic vs oxidative metabolism that adapted to their proliferating phenotype³¹. The ability of these cells to efficiently switch between metabolic pathways as environmental conditions change—demonstrated by the SCENITH technique—provides a significant advantage, especially when the availability of specific metabolites becomes constrained. In our *in vitro* model, Tregs are cultured in medium containing 17 mM glucose and in an incubator with 21% oxygen. These *in vitro* conditions change dramatically once Tregs are injected into patients where glucose concentration³² and oxygen partial pressure^{33,34} are significantly lower. When we analyzed metabolic capacities and dependencies of Tregs isolated from the spleen of mice 7 days after injection we found that mitochondrial dependence dramatically falls, suggesting a metabolism highly dependent on aerobic glycolysis. The superior

glycolytic capability of IL-7/15-Tregs, evidenced by an increase in glycolytic enzymes, enhanced glycolysis as measured by the Seahorse assay, and a higher rate of mitochondrial fission, suggests that these cells are well-equipped to thrive under the metabolic constraints encountered in the physiological environment. This preference for glycolysis, which has also been noted in intratumoral Treg cells, is further associated with changes in lipid metabolism towards synthesis³⁵ as indicated by the upregulation of transcription factors such as SREBPs in our transcriptomic data. This comprehensive metabolic reprogramming not only supports the proliferative demands of these cells but also underlines the metabolic flexibility that contributes to their enhanced performance *in vivo*. The use of glycolysis by Treg is controversial, since many publications showed that Treg metabolism is dominated by fatty acid oxidation and oxidative phosphorylation in physiological conditions³⁶. Tregs engage glycolytic metabolism only during initial activation, characterized by elevated GLUT1 expression and mTOR activity³⁷, although their suppressive capacity is then reduced. Moreover, glycolysis is highly active during Treg migration³⁸. Our experimental setting, in which naïve Treg were activated via TCR and cytokine stimulation closely resemble the one of initial activation and is therefore consistent with high rate of glycolysis. However, we do not see impairment of suppressive function, which was reported also by our group when Treg are grown with IL-7¹⁷. Our model of sustained induced proliferation with high concentration of cytokines is probably far from physiological Treg homeostasis and requires anabolic metabolism to meet the needs for *in vitro* expansion.

An increased capacity to survive *in vivo* was indeed associated to an advantage in terms of Treg persistence in NSG mice. Even though we observed differences in the suppressive activity of the two Treg products, in these experimental setting, all mice, even those treated with Tregs, developed GvHD like symptoms. Given the strength of the response against xeno-antigens we are planning to compare the effectiveness of Treg expanded with both the StM and the IL-7/15 M in other diseases such as models of autoimmune diabetes or protection of transplanted beta cell grafts.

In our research, we developed and utilized the IL-7/15M protocol to expand polyclonal Tregs from a highly purified naïve Tregs starting point. This represents a potential limit of our expansion protocol since in our cohort of adult donors the relative percentage of naïve Treg was approximately 10%. While achieving a final cell yield comparable to those reported in earlier clinical studies may be challenging with our data, the enhanced expansion, increased suppressive activity, and extended lifespan of Tregs could offset the lower infusion quantities. Moreover, the use of naïve Treg for therapeutic purposes is still debated. Some studies have reported that Treg freshly isolated from cord blood are 80% CD45RA⁺ and have weak suppressive function³⁹. However, after *in vitro* culture with antigenic stimulation suppressive function was rapidly acquired with no differences between Tregs isolated from cord blood and adult peripheral blood^{40,41}.

From a translational perspective, a further development of this project will be to adapt the expansion protocol to antigen specific Tregs, including TCR transgenic and CAR Tregs that are approaching to the experimental clinical phase^{9,42}. Given that an important barrier to a successful Treg therapy is related to the limited survival of infused Tregs, we propose a novel method for Treg expansion that confer better cell yield and expansion *in vivo*. We believe this method can be alternative to the ones based on high doses IL-2 to improve the survival and function of infused Tregs. A final general consideration is that *in vitro* culture conditions are substantially different from those cell will find once infused into patients. An *in vitro* culture period in which cells are progressively trained to adapt to *in vivo* conditions, such as reduction of glucose and oxygen, should be considered to reduce the impact on cell survival.

Material and methods

Cell isolation, purification, and FACS analysis

Sodium-heparinized peripheral venous blood samples derived from healthy donors who donate blood and were provided by the Immunohematology

and Transfusion Medicine Service of the San Raffaele hospital, Milan, Italy. Highly purified (98%) naïve/scm Treg were isolated using the FACS Aria II after staining with the following monoclonal antibodies from BD biosciences: CD4-PB (Clone SK3), CD25-APC-Cy7 clone (eBioDDR5), CD127-PE-CY7 (clone HIL-7R-M21), CD45RA-PE-Cy5 (clone HI-100), CD62L-PE (clone DREG-56), and CD95-APC (clone DX2) (Supplementary Fig. 1). According to the experimental needs STAT-5 phosphorylation was measured using anti STAT5 pY694 Alexa Fluor 647 (clone 47, BD Biosciences) and CD215 (alpha chain of the IL-15 receptor) was detected using anti CD215 APC (clone JM7A4, BD Biosciences). Apoptosis was induced using an agonistic anti CD95 monoclonal antibody (clone D2, BD Biosciences), and measured using an annexin V- propidium iodide staining kit from BD Biosciences.

In vitro expansion protocols

Sorted naïve Treg were plated at 5×10^4 /ml in 96-well U bottom plate (Thermo Fisher Scientific) with X-VIVO 15 medium (Lonza, catalog no. 04-418Q) containing 5% heat inactivated pooled fetal bovine serum (Sigma-Aldrich). In the standard method culture medium was supplemented with Dynabeads human T activator CD3/CD28 (Thermo Fisher) at a 1:1 bead/cell ratio, and 300 UI/ml rhIL-2 (Bio-Techne). In the IL-7/IL-15 method, rhIL-7 and rhIL-15 (R&D Systems) at 10 ng/ml were used instead of IL-2. Treg were cultured for 14 days and the culture medium and supplements were replaced at day 7 and 11.

Suppression assay

After expansion Treg were stained with eFluor 670 Cell Proliferation Dye and co-cultured with CFSE stained, FACS sorted, allogenic CD8 + T cells at 1:1, 1:2, 1:4, 1:8 and 1:0 Tcell:Treg ratios in the presence of anti CD3/CD28 beads at 1:10 cell/bead ratio. Cell culture was harvested at day 5 and the percentage of proliferating (CFSE diluted) T cells was calculated. The percentage of suppression was calculated as $100 - [100 \times (\text{percentage of proliferating cells with Treg present}) / (\text{percentage of proliferating cells without Treg present})]$.

Treg bio-energetic profiling, including SCENITH and Seahorse measurements

This protocol was adapted from the original SCENITH protocols developed by R. Argüello²⁷. Human T cells were incubated for 30 min at 37 °C, 5% CO₂ in 96 well plates in which we added antibodies for staining as described above followed by treatment for 15 min at 37 °C, 5% CO₂ with medium, 2-Deoxy-D-glucose (2DG, 100 mM; Sigma-Aldrich), oligomycin (1 µM; Sigma-Aldrich) or a combination of both drugs. Puromycin (10 µg/ml Abcam) was added for 30 min at 37 °C. Cells were subsequently fixed and permeabilized using the Foxp3 fixation/permeabilization kit (eBioscience) and intracellular staining of puromycin was performed using Click-iT™ Plus OPP Alexa Fluor™ 488 (Thermo-Fisher). Methods and formulas used to calculate capacities and dependencies are described in Supplementary Fig. 2.

SEAHORSE

StM-Treg and IL7/15-Treg were plated on Cell-Tak-coated Seahorse Bioanalyzer XFe24 culture plates (0.3 x 10⁶ cells/well) for Real-Time ATP rate assay. Experiments were performed twice and data presented is from two biological samples with four technical replicates. Cells were cultured in DMEM, pH 7.4, supplemented with 10 mM of glucose, 1 mM of pyruvate and 2 mM of glutamine; oligomycin (1.5 µM) and rotenone/antimycin A (0.5 µM, Merck) were added according to the protocol of the assay. Drugs were injected in a seahorse analyzer (Agilent) and OCR and ECAR data analyzed through the Wave software (Agilent).

Surrogate markers of oxidative phosphorylation and glycolysis were measured by flow cytometry using the following reagents according to the manufacturer's instructions. Mitochondrial cell mass was measured using the MitoTracker Green FM from Invitrogen-Molecular Probes. Glucose uptake was measured using 2-(N-(7-nitrobenz-2-oxa-,1,3-diazol-4-yl) amino)-2-deoxyglucose (2NBDG) from Life Technologies. L(+)-lactate

concentration was measured in the supernatants with a Lactate Assay Kit (Sigma-Aldrich).

RNA extraction, 3'-mRNA sequencing and analysis

Total RNA was extracted from large and small macrophages using the Single Cell RNA Purification Kit (Norgen Biotek), following the manufacturer's recommendations. Total RNA extracted from sorted macrophages were subjected to PolyA mRNA sequencing. Libraries were constructed by SMARTer v4 PLUS kit (Takara), according to manufacturer's instructions. Sequencing was performed with the NextSeq 500 (Illumina). All libraries were sequenced in single-end mode (75 bp length). Raw reads were preprocessed for adapter trimming and quality check was assessed using the FastQC tool (<http://www.bioinformatics.babraham.ac.uk/projects/fastqc>). Reads were aligned to the reference genome (GENCODE Homo sapiens release GRC38) using the STAR algorithm⁴³. Differential expression analysis was performed using the GLM approach implemented in the R/Bioconductor edgeR⁴⁴ package (R version 4.1.1; edgeR version 3.36). Sample correlation was estimated through Pearson correlation analysis. Results of differential analysis are provided in Supplementary files. The resulting gene lists were used as input for conducting Gene Ontology over-representation analysis with *enrichGO()* function from clusterProfiler (v4.2.2)⁴⁵.

Treg dynamic and modeling of xeno-GvHD in NSG mice

Female NOD/scid/IL-2Rc2/2 mice (NOD.cg-PrkdcscidIl2rgtm1Wjl/SzJ) abbreviated to NSG were obtained from The Jackson Laboratory and were used between 6–12 weeks of age. NSG mice were co-transplanted with 10⁷ PBMC and autologous 5×10^6 GFP+ StM-Treg or IL-7/15MTreg via the tail vein. Blood samples were collected to enumerate Treg and Tconv during follow-up. GvHD was monitored according to the score in Supplementary Fig. 4B. Animals that developed clinical symptoms of GvHD (15% weight loss, hunched posture, fur loss, reduced mobility, tachypnea) were sacrificed and an end point of survival was recorded for all mice. After 35 days mice were sacrificed and the spleen and liver were collected from survivors to detect the presence of T cell infiltrate.

Statistical analysis

Statistical analyses were performed using GraphPad Prism 9.0 software. Flow cytometry data were calculated as median fluorescence intensity (MFI) and subpopulations as percentage of positive cells. Proliferation was calculated as percentage of cells that diluted the fluorescent dye CFSE (% CFSEdim). Data were presented as mean ± standard deviation and the Wilcoxon matched paired t-test was used for comparisons of two groups. The Wilcoxon matched paired t-test with the Dunn-Bonferroni post-hoc test was used for comparisons when several t-test were calculated within the same experiment. Wilcoxon Rank Sum test (F) was used for comparisons of the enrichment scores (Fig. 2F). Kaplan-Meier survival curves were compared using the Log-rank (Mantel-Cox) test. A two-tailed *P* value of 0.05 was considered significant. The *P* value is indicated for each comparison or the following nomenclature was used: **P* < 0.05, ***P* < 0.01, ****P* < 0.001, ns, *P* > 0.05.

Study approval

Blood donors signed an informed consent in accordance with the D.M. November 2nd 2015 entitled "Provisions relating to the quality and safety requirements of blood components". In accordance with the ministerial provisions and the IOG 364 institutional procedure "Request and delivery of buffy coats for research purposes", it is not possible to retrieve any type of information (gender, age, HLA typing) of donors. The animal study protocol was approved by the local animal ethics committee of San Raffaele Hospital (IACUC n 532/2022-PR, approved September 12, 2022).

Reporting summary

Further information on research design is available in the Nature Portfolio Reporting Summary linked to this article.

Data availability

All Supplementary data are in Supplementary Data 1 file. The Treg RNA-Seq raw sequences are deposited in NCBI under BioProject ID PRJNA1190940. The data can be accessed via SRA Entrez (<https://www.ncbi.nlm.nih.gov/search/all/?term=PRJNA1190940>). The datasets used to create figures and analysis have been uploaded in accordance with the journal's requirements, and any data utilized and/or analyzed during this study are available at <https://doi.org/10.6084/m9.figshare.27929955>. All other data are available from the corresponding author on reasonable request.

Received: 22 July 2024; Accepted: 9 December 2024;

Published online: 21 January 2025

References

- Sakaguchi, S., Yamaguchi, T., Nomura, T. & Ono, M. Regulatory T cells and immune tolerance. *Cell* **133**, 775–787 (2008).
- Dikiy, S. & Rudensky, A. Y. Principles of regulatory T cell function. *Immunity* **56**, 240–255 (2023).
- Vignali, D. A. A., Collison, L. W. & Workman, C. J. How regulatory T cells work. *Nat. Rev. Immunol.* **8**, 523–532 (2008).
- Atif, M., Conti, F., Gorochov, G., Oo, Y. H. & Miyara, M. Regulatory T cells in solid organ transplantation. *Clin. Transl. Immunol.* **9**, 1–15 (2020).
- Guo, W. W. et al. Regulatory T Cells in GVHD therapy. *Front. Immunol.* **12**, 697854 (2021).
- Esensten, J. H., Muller, Y. D., Bluestone, J. A. & Tang, Q. Regulatory T-cell therapy for autoimmune and autoinflammatory diseases: the next frontier. *J. Allergy Clin. Immunol.* **142**, 1710–1718 (2018).
- Marek-Trzonkowska, N. et al. Administration of CD4+CD25highCD127-regulatory T cells preserves β -cell function in type 1 diabetes in children. *Diabetes Care* **35**, 1817–1820 (2012).
- Bluestone, J. A. et al. Type 1 diabetes immunotherapy using polyclonal regulatory T cells. *Sci. Transl. Med.* **7**, 315ra189 (2015).
- Tuomela, K. & Levings, M. K. Genetic engineering of regulatory T cells for treatment of autoimmune disorders including type 1 diabetes. *Diabetologia* **67**, 611–622 (2024).
- Ho, P. et al. Harnessing regulatory T cells to establish immune tolerance. *Sci. Transl. Med.* **16**, eadm8859 (2024).
- Gattinoni, L., Speiser, D. E., Lichterfeld, M. & Bonini, C. T memory stem cells in health and disease. *Nat. Med.* **23**, 18–27 (2017).
- Putnam, A. L. et al. Expansion of human regulatory T-cells from patients with type 1 diabetes. *Diabetes* **58**, 652–662 (2009).
- MacDonald, K. N., Piret, J. M. & Levings, M. K. Methods to manufacture regulatory T cells for cell therapy. *Clin. Exp. Immunol.* **197**, 52–63 (2019).
- Bayer, A. L. et al. A function for IL-7R for CD4 + CD25 + Foxp3 + T regulatory cells. *J. Immunol.* **181**, 225–234 (2008).
- Schmaler, M. et al. IL-7R signaling in regulatory T cells maintains peripheral and allograft tolerance in mice. *Proc. Natl Acad. Sci. USA* **112**, 13330–13335 (2015).
- Liu, W. et al. CD127 expression inversely correlates with FoxP3 and suppressive function of human CD4+ T reg cells. *J. Exp. Med.* **203**, 1701–1711 (2006).
- Heninger, A.-K. et al. IL-7 abrogates suppressive activity of human CD4+ CD25 + FOXP3+ regulatory T cells and allows expansion of alloreactive and autoreactive T cells. *J. Immunol.* **189**, 5649–5658 (2012).
- Vignali, D. et al. IL-7 mediated homeostatic expansion of human CD4+CD25+FOXP3+ regulatory T cells after depletion with anti-CD25 monoclonal antibody. *Transplantation* **100**, 1853–1861 (2016).
- Cosorich, I. et al. Interleukin-7 improves the fitness of regulatory T cells for adoptive transfer. *Immunology* **170**, 540–552 (2023).
- Gattinoni, L. et al. A human memory T cell subset with stem cell-like properties. *Nat. Med.* **17**, 1290–1297 (2011).
- Motwani, K. et al. Human regulatory T cells from umbilical cord blood display increased repertoire diversity and lineage stability relative to adult peripheral blood. *Front. Immunol.* **11**, 1–17 (2020).
- Argüello, R. J. et al. SCENITH: a flow cytometry-based method to functionally profile energy metabolism with single-cell resolution. *Cell Metab.* **32**, 1063–1075.e7 (2020).
- Lindqvist, L. M., Tandoc, K., Topisirovic, I. & Furic, L. Cross-talk between protein synthesis, energy metabolism and autophagy in cancer. *Curr. Opin. Genet. Dev.* **48**, 104–111 (2018).
- Aviner, R. The science of puromycin: from studies of ribosome function to applications in biotechnology. *Comput. Struct. Biotechnol. J.* **18**, 1074–1083 (2020).
- Dong, S. et al. The effect of low-dose IL-2 and Treg adoptive cell therapy in patients with type 1 diabetes. *JCI Insight* **6**, e147474 (2021).
- Cieri, N. et al. IL-7 and IL-15 instruct the generation of human memory stem T cells from naive precursors. *Blood* **121**, 573–584 (2012).
- Borghans, J. A. M., Tesselaar, K. & de Boer, R. J. Current best estimates for the average lifespans of mouse and human leukocytes: reviewing two decades of deuterium-labeling experiments. *Immunol. Rev.* **285**, 233–248 (2018).
- Hellerstein, M. K. et al. Subpopulations of long-lived and short-lived T cells in advanced HIV-1 infection. *J. Clin. Invest.* **112**, 956–966 (2003).
- Vukmanovic-Stejic, M. et al. Human CD4+CD25hiFoxp3+ regulatory T cells are derived by rapid turnover of memory populations in vivo. *J. Clin. Invest.* **116**, 2423–2433 (2006).
- Singh, K. et al. Superiority of rapamycin over tacrolimus in preserving non-human primate Treg half-life and Phenotype after adoptive transfer. *Am. J. Transplant.* **14**, 2691–2703 (2014).
- Procaccini, C. et al. The proteomic landscape of human ex vivo regulatory and conventional T cells reveals specific metabolic requirements. *Immunity* **44**, 406–421 (2016).
- Lu, W. et al. An atlas of glucose uptake across the entire human body as measured by the total-body PET/CT scanner: a pilot study. *Life Metab.* **1**, 190–199 (2022).
- Mizrahi, T., Morrison, J., Johnson, A. & Well, M. Oxygen saturation in the bone marrow of healthy volunteers. *Blood* **99**, 394 (2002).
- Wild, J. M. et al. 3D volume-localized pO2 measurement in the human lung with 3He MRI. *Magn. Reson. Med.* **53**, 1055–1064 (2005).
- Pacella, I. et al. Fatty acid metabolism complements glycolysis in th selective regulatory t cell expansion during tumor growth. *Proc. Natl Acad. Sci. USA* **115**, E6546–E6555 (2018).
- Tomaszewicz, M., Ronowska, A., Zieliński, M., Jankowska-Kulawy, A. & Trzonkowski, P. T regulatory cells metabolism: the influence on functional properties and treatment potential. *Front. Immunol.* **14**, 1–11 (2023).
- Gerriets, V. A. et al. Foxp3 and toll-like receptor signaling balance T reg cell anabolic metabolism for suppression. *Nat. Immunol.* **17**, 1459–1466 (2016).
- Kishore, M. et al. Regulatory T cell migration is dependent on glucokinase-mediated glycolysis. *Immunity* **47**, 875–889.e10 (2017).
- Fujimaki, W. et al. Comparative study of regulatory T cell function of human CD25+ CD4+ T cells from thymocytes, cord blood, and adult peripheral blood. *Clin. Dev. Immunol.* **2008**, 305859 (2008).
- Santner-Nanan, B. et al. Accelerated age-dependent transition of human regulatory T cells to effector memory phenotype. *Int. Immunol.* **20**, 375–383 (2008).
- Thornton, C. A. et al. Functional maturation of CD4+CD25+CTLA4+ CD45RA+ T regulatory cells in human neonatal T cell responses to environmental antigens/allergens. *J. Immunol.* **173**, 3084–3092 (2004).
- Doglio, M. et al. Regulatory T cells expressing CD19-targeted chimeric antigen receptor restore homeostasis in Systemic Lupus Erythematosus. *Nat. Commun.* **15**, 2542 (2024).

43. Dobin, A. et al. STAR: ultrafast universal RNA-seq aligner. *Bioinformatics* **29**, 15–21 (2013).
44. Robinson, M. D., McCarthy, D. J. & Smyth, G. K. edgeR: a bioconductor package for differential expression analysis of digital gene expression data. *Bioinformatics* **26**, 139–140 (2009).
45. Yu, G., Wang, L. G., Han, Y. & He, Q. Y. ClusterProfiler: an R package for comparing biological themes among gene clusters. *OMICS J. Integr. Biol.* **16**, 284–287 (2012).

Acknowledgements

Juvenile Diabetes Research Foundation grant 2-SRA-2021-1002-S-B (P.M.). EFSD/JDRF/Lilly European Program in Type 1 Diabetes Research (P.M.). Fondazione Italiana Diabete (FID) (P.M.).

Author contributions

Conceptualization: P.M. Methodology: J.F., A.F., T.J., A.P., S.C., and F.B. Investigation: J.F., A.F., T.J., A.P., F.B., S.C., C.D.D., F.M., G.D.N., C.B., L.P., and P.M. Visualization: J.F., A.F., T.J., A.P., F.B., S.C., C.D.D., F.M., G.D.N., C.B., L.P., and P.M. Funding acquisition: P.M. Project administration: P.M. Supervision: F.M., G.D.N., F.B., C.B., L.P., and P.M. Writing—original draft: A.F., F.M., G.D.N., F.B., C.B., L.P., and P.M.

Competing interests

The authors declare no competing interests.

Additional information

Supplementary information The online version contains supplementary material available at <https://doi.org/10.1038/s42003-024-07381-1>.

Correspondence and requests for materials should be addressed to Paolo Monti.

Peer review information *Communications Biology* thanks Nimi Marcel and the other, anonymous, reviewer for their contribution to the peer review of this work. Primary Handling Editor: Mengtan Xing. A peer review file is available.

Reprints and permissions information is available at <http://www.nature.com/reprints>

Publisher's note Springer Nature remains neutral with regard to jurisdictional claims in published maps and institutional affiliations.

Open Access This article is licensed under a Creative Commons Attribution-NonCommercial-NoDerivatives 4.0 International License, which permits any non-commercial use, sharing, distribution and reproduction in any medium or format, as long as you give appropriate credit to the original author(s) and the source, provide a link to the Creative Commons licence, and indicate if you modified the licensed material. You do not have permission under this licence to share adapted material derived from this article or parts of it. The images or other third party material in this article are included in the article's Creative Commons licence, unless indicated otherwise in a credit line to the material. If material is not included in the article's Creative Commons licence and your intended use is not permitted by statutory regulation or exceeds the permitted use, you will need to obtain permission directly from the copyright holder. To view a copy of this licence, visit <http://creativecommons.org/licenses/by-nc-nd/4.0/>.

© The Author(s) 2025, corrected publication 2025